Geophysical Journal International

Geophys. J. Int. (2015) **203,** 475–481
GJI Gravity, geodesy and tides

doi: 10.1093/gji/ggv312

Decadal and quadratic variations of Earth's oblateness and polar ice mass balance from 1979 to 2010

Ki-Weon Seo,[1] Jianli Chen,[2] Clark R. Wilson[2,3] and Choon-Ki Lee[4]

[1] *Department of Earth Science Education, Seoul National University, Seoul,* 151-742*, Republic of Korea. E-mail: seokiweon@snu.ac.kr*
[2] *Center for Space Research, University of Texas at Austin, TX* 78759*, USA*
[3] *Department of Geological Sciences, Jackson School of Geosciences, University of Texas at Austin, TX* 78712*, USA*
[4] *Division of Polar Earth System Sciences, Korea Polar Research Institute, Incheon,* 406-840*, Republic of Korea*

Accepted 2015 July 23. Received 2015 July 21; in original form 2015 March 4

SUMMARY

Gravity variations associated with Earth's oblateness (J_2) have been observed by satellite laser ranging (SLR) since 1976. The J_2 time-series has been used to measure and help understand many geophysical processes within the Earth system ranging from the mantle to the atmosphere. While post glacial rebound and the Earth climate system are believed to be the primary driving forces of long-term and seasonal J_2 variations, the physical cause of decadal and longer timescale J_2 variations has remained uncertain, although recent evidence indicates that polar ice mass changes are important. In this study, we estimate a variety of climate contributions to J_2 over the period 1979–2010, and find that ice mass variations in Greenland and Antarctica are the dominant cause of observed decadal and longer J_2 variations. Residual variations at periods near 10–11 years may reflect limitations of numerical climate models in estimating mass change variability at long periods, but are also suggestive of potential contribution related to variable solar activity.

Key words: Satellite geodesy; Time variable gravity; Global change from geodesy.

1 INTRODUCTION

One of the most prominent features in Earth's shape is the equatorial bulge, mainly a consequence of Earth's rotation. This oblateness of Earth produces the largest departure of Earth's gravity from that of a spherically symmetric body, and is measured by the J_2 (degree 2, order 0) coefficient of gravity in a spherical harmonic representation. J_2 changes over a broad spectrum of timescales, ranging from tidal to seasonal to the age of the Earth. The range of associated physical causes implies that J_2 variations are a useful global measure of large-scale mass redistribution within the Earth system.

J_2 variations have been measured by satellite laser ranging (SLR) since 1976, starting with the launch of LAGEOS. The dominant elements of the J_2 time-series are a negative trend with superimposed seasonal variability. The negative trend indicates that Earth is becoming less oblate, mostly due to Post Glacial Rebound (PGR; Yoder *et al.* 1983) and polar ice mass loss (Nerem & Wahr 2011). Seasonal variations reflect redistribution of air and water mass between tropical and extra-tropical regions (Gutierrez & Wilson 1987). As longer J_2 time-series became available, interannual and decadal signals were revealed. These timescales are likely to be climate-related, possibly tied to glacier melting, variations such as the El Niño-Southern Oscillation (ENSO) and the Pacific Decadal Oscillation (PDO), or to the 18.6-yr ocean tide (Cox & Chao 2002; Dickey *et al.* 2002; Cheng & Tapley 2004).

Recently, Cheng *et al.* (2013) examined J_2 variations from 1976 to 2011 and suggested that accelerating ice mass loss from glaciers and ice sheets is probably one of the causes that may explain long-term variations. Nerem & Wahr (2011) showed that J_2 variations can be largely explained by polar ice mass changes from 2002 to 2010 based on GRACE observations over Greenland and Antarctica. A remaining question is accounting for J_2 variations in the pre-GRACE era. A main problem has been limitations of both observations and models of climate-related mass redistribution. This is particularly true for polar region where long-term ice mass changes have been poorly observed over a large part of the nearly four-decade span of the J_2 time-series prior to GRACE. Here we investigate a variety of sources, especially those related to Greenland and Antarctic ice mass changes for the period 1979–2010. J_2 comparison between observations and models should be useful to validate the estimate of polar ice mass changes as well as to understand earth oblateness variations for the last four decades.

J_2 variations (ΔJ_2) are estimated from multiple satellite SLR observations (Cheng *et al.* 2013), and are available from the GRACE Tellus website (http://grace.jpl.nasa.gov/data/j2). ΔJ_2 is given at 30-d intervals, and is resampled here to monthly values (centered in the middle of the month) to compare with monthly climate model series (Fig. 1a). Since causes of the linear trend and seasonal variations are relatively well known (Yoder *et al.* 1983; Gutierrez & Wilson 1987; Nerem & Wahr 2011), our examination focuses on interannual and longer variations by removing the linear trend and seasonal terms

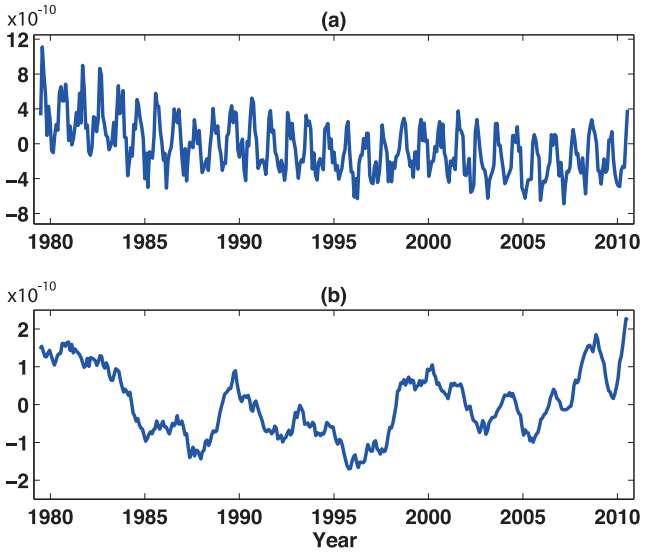

Figure 1. (a) Time-series of ΔJ_2 and (b) residual time-series of ΔJ_2 after removing linear trends and seasonal cycles by least squares.

from ΔJ_2. In addition, we apply an 11-month moving average to suppress high frequencies in the residual ΔJ_2. The resulting time-series of ΔJ_2 is dominated by interannual, decadal and quadratic variations (Fig. 1b). In the next section, we develop estimates of various climate-related contributions in order to explain variations in Fig. 1(b).

2 CLIMATE CONTRIBUTIONS TO ΔJ_2

Change of surface mass density, $\Delta\sigma(\theta, \phi)$, driven by geophysical or climate variations alter J_2, and can be calculated by integration over Earth's surface (Chao *et al.* 1987):

$$\Delta J_2 = -\frac{1+k_2}{5}\frac{R_e^2}{M_e}\int \Delta\sigma(\theta,\phi)P_2(\cos\theta)\,\mathrm{d}S \qquad (1)$$

in which $k_2 = -0.303$ is the Earth's degree 2 load Love number (Han & Wahr 1995), R_e and M_e are the mean radius and mass of the Earth, respectively. $P_2(\cos\theta)$ is the Legendre polynomial (spherical harmonic), and θ and ϕ are latitude and longitude, respectively. To calculate ΔJ_2, we use $\Delta\sigma(\theta, \phi)$ from multiple climate models and observations.

We estimate continental water contributions to ΔJ_2 using the Global Land Data Assimilation System Version 2 (GLDAS-2) (Rodell *et al.* 2004), available from 1948 to 2010. GLDAS-2 is forced by a climatologically consistent data set whereas forcing in the earlier version (GLDAS-1) created spurious trends, making it unsuitable for long-term terrestrial water estimates (Rui & Beaudoing 2013). In addition, contemporary hydrology models are probably inadequate to understand long-term terrestrial water variations since they are designed to maintain long-term water balance. As a result, Cheng *et al.* (2013) excluded continental water variations in their ΔJ_2 study. Here we use only soil moisture contribution to ΔJ_2. The ERA-Interim surface pressure field (Simmons *et al.* 2007) is used for terrestrial atmospheric mass variations including Greenland and Antarctica. For ocean mass variations (bottom pressure), we combine ERA-Interim surface pressure with an inverted barometer assumption and ocean mass redistribution from GECCO (German partner of the Estimating the Circulation and Climate of the Ocean; Stammer *et al.* 2004). GECCO is forced by NCEP fields available from 1952 to 2011. GECCO is used in place of ECCO

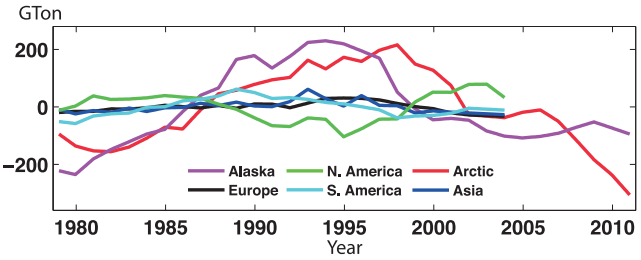

Figure 2. Glacier mass balance on the continents including Alaska. Linear trends are removed.

which depends upon assimilated satellite altimeteric observations starting in 1992. Because GECCO does not conserve mass, mass conservation is imposed here by removing changes in mean ocean mass every month. Seasonal cycles and linear trends are removed from soil moisture, surface pressure and ocean bottom pressure time-series.

Mountain glacier contributions are estimated using glacier mass balance data (Dyurgerov 2002) from the National Snow & Ice Data Center (NSIDC) (http://nsidc.org/data/G10002). Annual mountain glacier mass balance rates are available from 1961 to 2003. Fig. 2 shows the detrended cumulative continental glacier mass balance rate from 1979 to 2003 including Alaska. The time-series for Alaska and the Arctic is extended to 2010 using GRACE Release 5 (RL05) solutions provided by the Center for Space Research, University of Texas at Austin. Leakage bias due to the limited degree and order of GRACE spherical harmonics and spatial filtering is corrected using unconstrained global forward modelling (Chen *et al.* 2014). Glacier effects from other regions might also be estimated using GRACE, but the task is more difficult due to spatial leakage from adjacent hydrologic signals. There is some indication that mountain glacier storage in other areas is more stable (Jacob *et al.* 2012). In addition, glacier contributions from mid-latitudes, where the degree 2 order 0 spherical harmonic is small, would have a diminished effect on ΔJ_2. Thus we include only Alaska and Arctic glacier effects on ΔJ_2. ΔJ_2 comparisons between Alaska/Arctic glaciers and other area are shown below.

Polar ice mass variations from 1979 to 2010 are estimated from climate models and satellite observations. These changes can be separated into effects of surface mass balance (*SMB*) and ice discharge (*D*),

$$\begin{aligned}\Delta M_{T_0}^{T}(\theta,\phi) &= \int_{T_0}^{T} SMB(\theta,\phi)\,\mathrm{d}t - \int_{T_0}^{T} D(\theta,\phi)\,\mathrm{d}t \\ &= \int_{T_0}^{T}(P(\theta,\phi) - R(\theta,\phi))\,\mathrm{d}t - \int_{T_0}^{T} D(\theta,\phi)\,\mathrm{d}t \qquad (2)\end{aligned}$$

SMB depends on the difference between precipitation (*P*) and runoff (*R*). We ignore minor components of ice mass balance such as sublimation (Lenaerts *et al.* 2012) and basal melting of grounded ice. We remove linear trends and seasonal terms from each component of eq. (2). The time integrated residuals (denoted by $_*$) are related by

$$\Delta M_* = P_* - R_* - D_*, \qquad (3)$$

where ΔM_*, P_*, R_* and D_* are residual ice mass changes and accumulations of precipitation, meltwater runoff and ice discharge, respectively. We use a regional climate model, RACMO2 (van Angelen *et al.* 2012) for P_*-R_* in Greenland. In Antarctica, R_* is nearly zero because surface melting and rainfall are minor and refrozen in snowpack (van Wessem *et al.* 2014). Therefore, for *SMB*

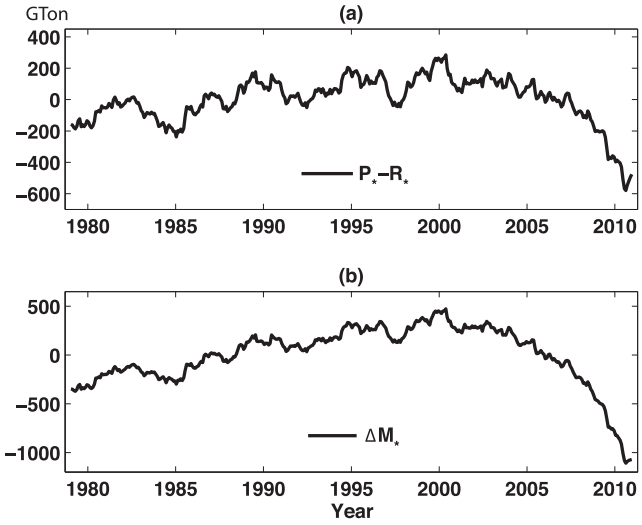

Figure 3. (a) Anomalous surface mass balance (P_*-R_*) accumulation (after removing seasonal cycles and linear trends) and anomalous ice mass balance (ΔM_*) including surface mass balance and ice discharge in Greenland.

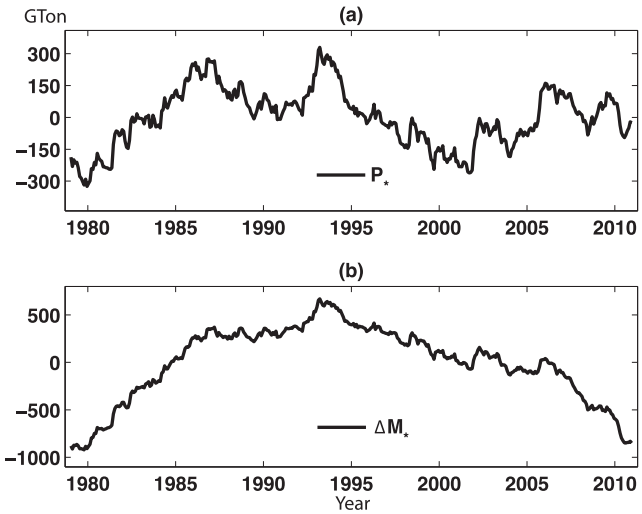

Figure 4. (a) Anomalous surface mass balance (P_*) accumulation (after removing seasonal cycles and linear trends) and ice mass balance (ΔM_*) including surface mass balance and ice discharge in Antarctica.

in Antarctica, we only use ERA-Interim precipitation results (Simmons *et al.* 2007). Medley *et al.* (2013) found that reanalysis precipitation variations agree better with in-situ data than the regional climate model estimates in Antarctica. In addition, ERA-Interim is superior among contemporary global reanalysis in estimating precipitation change at high southern latitudes (Bromwich *et al.* 2011). Figs 3(a) and 4(a) show Greenland P_*-R_* and Antarctic P_*, respectively.

There are limited observations and models of D_* which is a measure of departures of ice discharge from a constant rate. These would reflect changing ice dynamics, including acceleration of discharge over time. Long-term (1958–2007) annual ice discharge in Greenland was reported in Rignot *et al.* (2008b): East and west Greenland experienced ice discharge increases during the last two decades while ice discharge variation in the east was stable from 2005 to 2007. Similar ice discharge variations were examined for 2000–2012 (Enderlin *et al.* 2014): In the west, ice discharge has increased about 3 GTon yr^{-1} since 2000, and in the southeast, it increased from 2000 to 2004 and has been stable since 2005. For D_* from 1979 to 2010, we combine ice discharge estimates from both studies of Rignot *et al.* (2008b) and Enderlin *et al.* (2014). Fig. 3(b) shows ΔM_* ($= P_*-R_*-D_*$) in Greenland. Evident ice mass loss acceleration occurred during the last decade resulting mainly from similar acceleration in P_*-R_* (Sasgen *et al.* 2012; Seo *et al.* 2015a).

Several studies also showed that ice discharge has increased in the Antarctic Peninsula (AP) and Amundsen Sea Sector (AS; Rignot *et al.* 2008a). Mouginot *et al.* (2014) estimated the annual ice discharge based on Landsat and satellite radar interferometry from 1974 to 2013. Most recently, Seo *et al.* (2015b) also quantified D_* in AS and AP from 2003 to 2013 based on GRACE observation accounting for *SMB* variations and atmospheric pressure errors. The two D_* estimates in AS are remarkably similar to each other during the common period (Seo *et al.* 2015b), and thus we use D_* in AS from the estimates by Mouginot *et al.* (2014). Unlike in AS, detailed ice discharge variations in AP during the last three decades have not been reported yet. However, Seo *et al.* (2015b) showed that the acceleration rate in AP D_* is about 5.0 GTon yr^{-2}, corresponding to coefficient a_1 in a least square fit of the form $a_0 + a_1\frac{1}{2}(t-t_0)^2$ to D_*, where t_0 is the middle of the given period. Rignot *et al.* (2008a) also showed that the AP ice discharge increased from 107 to 136 GTton yr^{-1} during 10 yr (1996–2006), equivalent to the acceleration rate of about 5.8 GTon yr^{-2}, which is very close to the GRACE-based study. Therefore, for D_* in AP, we use the acceleration (quadratic) component, 5.0 GTon yr^{-2}, for the entire period (1979–2010) under the reasonable assumption that Antarctic ice dynamic variations have long (decadal) timescales. Fig. 4(b) shows $\Delta M_* = P_*-D_*$ in Antarctica.

A final step in the calculation is to enforce water mass conservation for the globe by computing the terrestrial mass anomaly from all effects (soil moisture, mountain glaciers and ice sheets). Ocean mass is adjusted by this amount, by adding or subtracting a uniform layer of water. Although the spatial pattern of the adjusted ocean mass is not uniform due to the nature of self-gravitation of fluid on Earth's envelope (Farrell & Clark 1976), this procedure considers the first order water mass redistribution between land and oceans.

3 ΔJ_2 COMPARISON BETWEEN MODEL AND OBSERVATION

Fig. 5(a) shows observed (blue from Fig. 1b) and estimated (black, green and magenta) ΔJ_2 representing effects of surface pressure, ocean bottom pressure and soil moisture, respectively. Fig. 5(a) suggests correlation of higher frequency oscillations particularly for surface pressure, but longer period variations differ. Fig. 5(b) shows observed (blue) and estimated (black and magenta) ΔJ_2 associated with mountain glaciers. The black line shows ΔJ_2 for Alaska and Arctic glaciers, and magenta line exhibits ΔJ_2 for other glaciers. Alaska and Arctic glaciers contribute some decadal and longer variations of ΔJ_2 while others do not affect ΔJ_2. Fig. 5(c) includes Greenland ice mass balance (ΔM_*) (black). Estimated ΔJ_2 from Greenland ice mass balance shows similar long-term variability to the observed ΔJ_2 (blue). In particular, the recent ΔJ_2 increase starting at about 2005 is largely associated with Greenland ice mass balance. Fig. 5(d) is similar to Fig. 5(c) except the black line here is for Antarctic ice mass balance. The long-term parabolic shape exhibited by the blue line is largely explained by Antarctic ice mass balance, indicating that long-term variation of earth oblateness

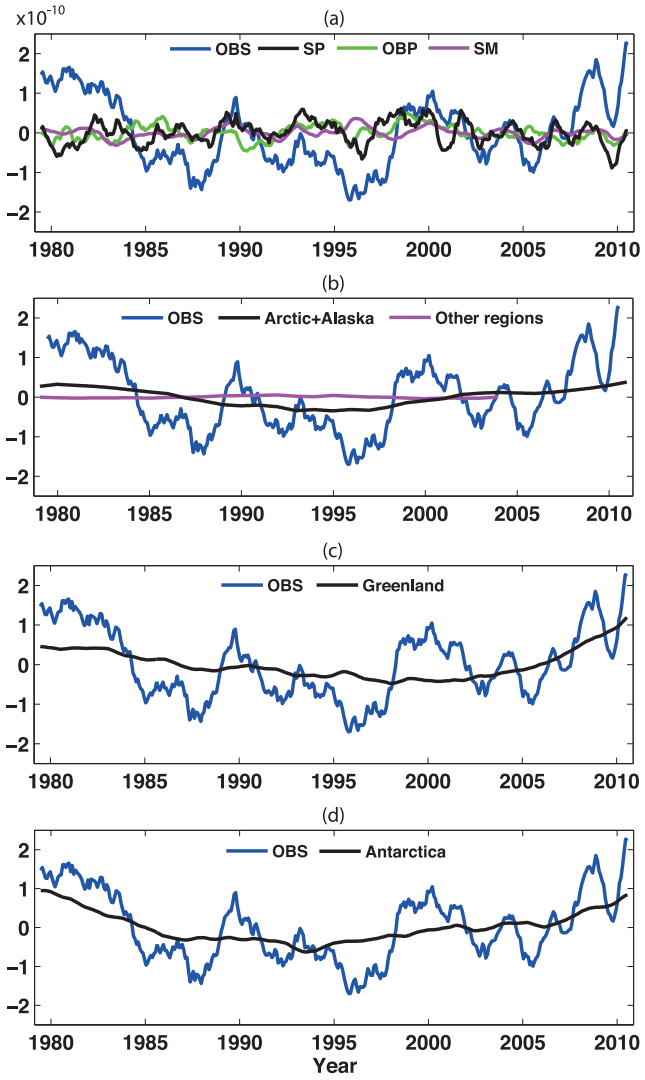

Figure 5. Comparison between observed (blue) and modelled ΔJ_2. For ΔJ_2 calculations, geophysical models include (a) surface pressure (black, SP), ocean bottom pressure (green, OBP) and soil moisture (magenta, SM), (b) mountain glacier mass balance in Alaska and Arctic (black) and other regions (magenta), (c) ice mass balance in Greenland (black) and (d) ice mass balance in Antarctica (black).

during the last four decades is mainly associated with ice mass loss acceleration in Antarctica.

Results shown in Fig. 5 imply that Greenland and Antarctic ice mass balance is a major cause of long-term and decadal ΔJ_2 variations while higher frequency variations result mostly from atmospheric pressure. Now we combine all climate components to compare with ΔJ_2 observations. Fig. 6 shows observed (blue) and estimated (red) ΔJ_2, the combined effect of surface pressure, ocean bottom pressure, soil moisture, mountain glaciers and polar ice sheets. Now the two time-series agree remarkably with each other (with a correlation coefficient $r = 0.86$, and p-value is close to zero). Excellent correlation and comparable magnitudes indicate that long-term global mass redistribution estimates used here are reasonably accurate. This is particularly important because they imply a good estimate of the pre-GRACE history of ice mass balance in polar regions, potentially useful for projecting future sea level variations. Blue and red numbers in the figure represent the acceleration coefficients (2nd order polynomial coefficient) for observations and model estimate, respectively. The two acceleration rates also agree with each other within the stated uncertainty, which corresponds to a 95 per cent confidence interval considering polynomial misfit with a conventional assumption of normally distributed independent residuals.

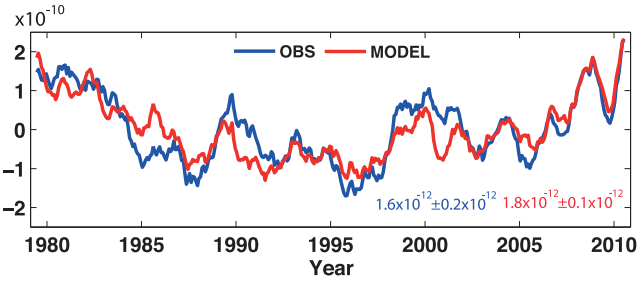

Figure 6. Comparison between modelled (red) and observed (blue) ΔJ_2. Modelled ΔJ_2 includes contributions from soil moisture, atmospheric and ocean bottom pressure, and mountain glacier and polar ice sheet mass balance.

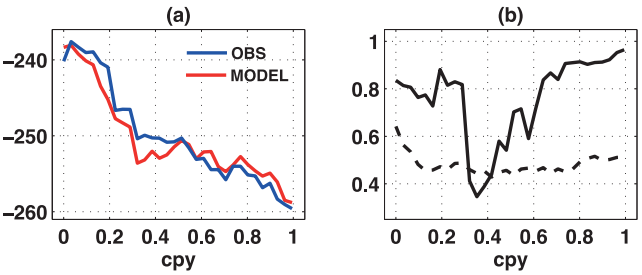

Figure 7. (a) Power spectra of observed (blue) and modelled (red) ΔJ_2. The vertical scale is in decibels. (b) Coherence between modelled and observed ΔJ_2 (solid black) and its 95 per cent uncertainty level (dash black).

Although Fig. 6 shows good agreement between observation and model estimates, there are some differences. In particular, an abrupt ΔJ_2 increase is observed in 1998 but is only partly present in the model ΔJ_2. Chao *et al.* (2003) found a similar result and suggested that ocean models do not properly simulate water mass redistribution at long periods, in particular those associated with the PDO. Similar disagreements between modelled and observed ΔJ_2 are also found during 1985–1987 and 1990–1992. Overall, amplitude differences between observed and modelled ΔJ_2 suggest underestimation of modelled ΔJ_2 in the presence of otherwise similar temporal variability.

The correlation coefficient ($r = 0.86$) is a broad-band measure of correlation, but it is also possible to analyze correlation as a function of frequency using power spectra and coherence analysis. Fig. 7(a) shows the power spectra of observed and modelled ΔJ_2 using a multitaper (six taper) method. Since seasonal cycles are removed and an 11-months moving average is applied, frequencies above 1 cycle per year (cpy) are not of interest. There are 32 spectrum values between 0 and 1 cpy (nominal bandwidth of 0.03 cpy), but the bandwidth of each estimate is 0.19 cpy, due to spectral smoothing associated with the 6 tapers. The two power spectra are similar to each other except around 0.35 cpy (~3 year period) where the model power spectrum falls below the observed by about 3 decibels, suggesting that the model lacks a signal important in this frequency range. Fig. 7(b) exhibits the coherence spectrum as a companion to the power spectra in Fig. 7(a). A 95 per cent confidence level for significant coherence is estimated by a Monte Carlo method (1000 trials) which takes into account the non-white nature of the power spectra, and the duration of the time-series. The solid black line in

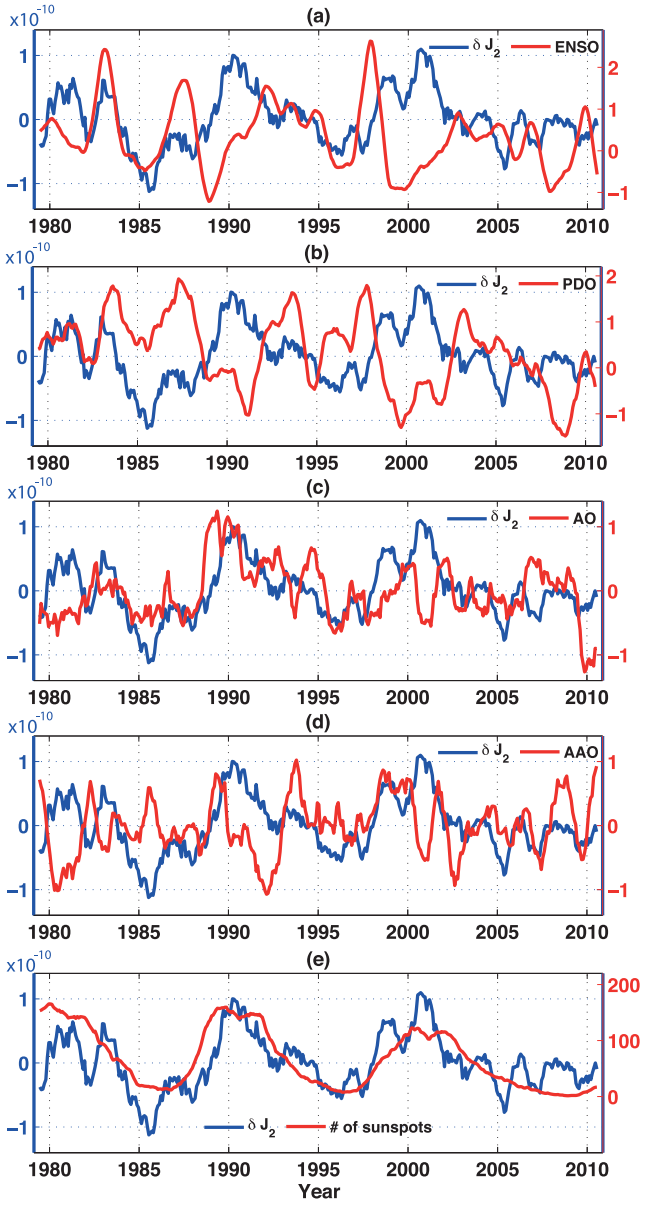

Figure 8. (a–d) Comparison between δJ_2 (blue), the difference between observed and modelled ΔJ_2, and climate indices (red). (e) Similar plot to (a–d) except that the red line is the number of sunspots.

Fig. 7(b) shows the coherence, and the dashed black line represents the 95 per cent confidence level. The coherence is significant except near 0.35 cpy as indicated in Fig. 7(a). This suggests a missing component in the model time-series, and it is consistent with the appearance of observed and modelled ΔJ_2 in Fig. 6 that shows some differences at interannual timescale.

Fig. 8 shows (in blue) the residual δJ_2, the difference between observed and modelled ΔJ_2 (shown in Fig. 6). We interpret δJ_2 as reflecting both limitations of climate model estimates (Chao *et al.* 2003) and possibly long-term geodetic variations of other origins (Cheng *et al.* 2013). Figs 8(a)–(d) compare δJ_2 with several climate indices (in red), including ENSO, PDO, AO and AAO, respectively. It appears that climate indices correlate with δJ_2 during particular time spans. For example, ENSO and PDO indices show opposite variations to δJ_2 during 1998–2010. In general, variations of the AO index and δJ_2 are similar to each other during 1983–1998, and those between AAO and δJ_2 are opposite during 1979–1988. The suggestion from Fig. 8 is that multiple climate oscillations may affect earth oblateness, but it is difficult to be more definite without further investigation of how well these climate oscillation signals are represented in the climate model predictions.

The residual δJ_2 also shows apparent oscillations with a period near 10-yr. Cheng & Tapley (2004) also found a similar period (∼10.6-yr) in J_2 based on wavelet decomposition. Solar activity (measured by the number of sunspots) varies with an 11-yr period, as shown by the red line of Fig. 8(e) after applying an 11-month moving average as done to ΔJ_2. There appears to be correlation with δJ_2 over most of 1979–2010, especially since the early 1980s. In addition, δJ_2 appears to track the recent unusual solar minimum of 2008 (Russell *et al.* 2010), which was delayed from the expected year of 2006. Since solar irradiance is very stable during the course of a solar cycle, it is not likely that solar activity has contaminated SLR solutions by variation of solar radiation pressure (John Ries, University of Texas at Austin, personal communication). Another suggestion that might be taken from Fig. 8(e) is that solar activity influences Earth's climate (Meehl *et al.* 2009), altering air or water mass redistribution in some fashion not yet incorporated in climate models. In the analysis here, we used GLDAS-2 and GECCO for land and ocean mass redistribution, respectively. These models may have limited skill in representing climate variations associated with the approximately 11-yr solar cycle.

It is also possible that decade-scale components of δJ_2 may be related to the lunar nodal tides at 18.6- and 9.3-yr periods, but while δJ_2 in Fig. 8 shows oscillations near a period of 10 yr, an 18.6-yr variation is not evident. The 9.3-yr tide is about 30 times smaller than the 18.6-yr tide (Cheng & Tapley 2004), so it would be an unlikely explanation for the ∼10-yr variation seen in δJ_2.

Earlier studies by Cheng & Tapley (2004) and Cheng *et al.* (2013) noted variations near the 18.6-yr period in their residual J_2 time-series. They discussed as possible causes ocean tides and anelastic mantle response for long-period ocean loading. A similar residual is not apparent in our δJ_2, and we show here that climate contributions in our model time-series have accounted for these rather than ocean tides. We first replicate the residual time-series given by Cheng *et al.* (2013). Observed ΔJ_2 time-series from January 1976 to May 2010 are decomposed using a level 7 'dmey' wavelet as in their study. A quadratic fit is removed from the decomposed time-series, and the result is shown in the dashed blue line of Fig. 9(a). This is identical to the dashed blue line of Fig. 2 in Cheng *et al.* (2013). The same wavelet decomposition is applied to observed ΔJ_2 (blue line in Fig. 6) from January 1979 to December 2010, and the quadratic fit is removed from the decomposed time-series. The two wavelet decomposed time-series exhibit large amplitude difference while their phases are similar. Amplitude differences are probably due to the different lengths of time-series and data reduction before applying the wavelet decomposition. Prior to the wavelet transform, here we remove linear trends and seasonal cycles from observed and modelled ΔJ_2 while Cheng *et al.* (2013) retained linear trend and seasonal terms. The solid red line shows a similar time-series to the solid blue line except that wavelet decomposition is applied to our model ΔJ_2 (red line in Fig. 6). The two time-series show similar variations, about two cycles during the period 1979–2010. This confirms that the apparent 18.6-yr oscillation is not associated with ocean tides but instead is explained by climate phenomena because model ΔJ_2 does not include any effect from tides. Fig. 9(b) shows that these variations are probably associated with Alaska and Arctic glaciers. The red line shows ΔJ_2 contributions from Alaska and Arctic glaciers after a 2nd-order polynomial fit is removed.

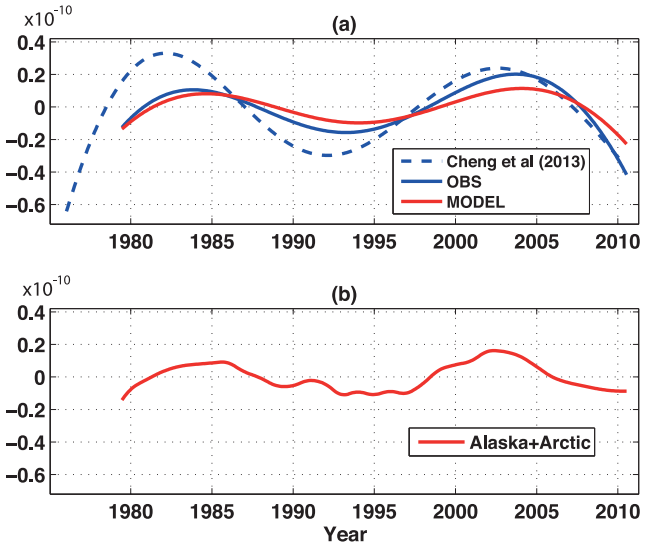

Figure 9. (a) A wavelet decomposition of time-series: observed ΔJ_2 shown in Cheng *et al.* (2013) (dashed blue), observed ΔJ_2 used in this study (solid blue) and modelled ΔJ_2 (solid red). (b) ΔJ_2 from mountain glacier mass balance in Alaska and Arctic. Quadratic terms are removed.

About two cycles of an oscillation are apparent from 1979 to 2010, with phase and amplitude similar to the solid red line in Fig. 9(a). The conclusion is that an ocean tidal source for the apparent 18.6-yr variation in ΔJ_2 is unlikely, but decadal variations of glacier mass balance are a likely cause of the apparent long-period oscillation in ΔJ_2.

4 CONCLUSIONS

Predictions of Earth dynamic oblateness changes (ΔJ_2) from geophysical models (atmosphere, hydrosphere and cryosphere) agree reasonably well with ΔJ_2 variations observed by SLR. Nerem & Wahr (2011) found that polar ice mass balance was an important contributor to long-term change of ΔJ_2 during the GRACE era. Cheng *et al.* (2013) examined ΔJ_2 variation before the GRACE era but the results were limited in accounting for ΔJ_2 without estimates of interannual and longer ice mass changes in Greenland and Antarctica over most of the SLR observation period. By combining model estimates and observations, we can reconstruct previous polar ice mass balance from 1979 to 2010, and it now is clear that Greenland and Antarctic ice mass variations are the main driving forces of long-term ΔJ_2 variations during the last four decades. This is potentially important because polar ice mass variations were poorly understood before the GRACE era. An extended multidecadal polar ice mass variation estimate should be useful for sea level forecasts.

It has been suggested that ΔJ_2 would include effects of the 18.6 yr tide (Cheng & Tapley 2004). While a variation near this period is present in the observed time-series, Alaska and Arctic glacier mass change mostly account for it. Residual δJ_2 variations show a clear oscillation near 10–11 yr. Correlations with the sunspot time-series are intriguing, suggesting some connection with solar activity. This connection might be through climate-related variations of mass redistribution which alter Earth's J_2, or other unknown causes. Further investigation is needed to better understand the cause of the 10–11 yr residual δJ_2 variations and connections with the solar cycle.

ACKNOWLEDGEMENTS

This work was supported by Korean national research foundation grant NRF-2013R1A1A2008368 and Korea Polar Research Institute (KOPRI) research grant PM15020. Chen and Wilson were supported by NASA GRACE Science Program (NNX12AJ97G), NASA ESI Program (NNX12AM86G) and NSF OPP Program (ANT-1043750).

REFERENCES

Bromwich, D.H., Nicolas, J.P. & Monaghan, A.J., 2011. An assessment of precipitation changes over Antarctica and the Southern Ocean since 1989 in contemporary global reanalyses, *J. Climate,* **24,** 4189–4209.

Chao, B.F., O'Connor, W.P., Chang, T.C., Hall, D.K. & Foster, J.L., 1987. Snow-load effect on the Earth's rotation and gravitational field, 1979–1985, *J. geophys. Res.,* **92,** 9415–9422.

Chao, B.F., Au, A.Y., Boy, J.-P. & Cox, C.M., 2003. Time-variable gravity signal of an anomalous redistribution of water mass in the extratropic Pacific during 1998–2002, *Geochem. Geophys. Geosyst.,* **4**(11), 1096, doi:10.1029/2003GC000589.

Chen, J., Li, J., Zhang, Z.Z. & Ni, S.N., 2014. Long-term groundwater variations in Northwest India from satellite gravity measurements, *Global planet. Change,* **116,** 130–138.

Cheng, M. & Tapley, B.D., 2004. Variations in the Earth's oblateness during the past 28 years, *J. geophys. Res.,* **109,** B09402, doi:10.1029/2004JB003028.

Cheng, M., Tapley, B.D. & Ries, J.C., 2013. Deceleration in the Earth's oblateness, *J. geophys. Res.,* **118,** 740–747.

Cox, C.M. & Chao, B.F., 2002. Detection of a large-scale mass redistribution in the terrestrial system since 1998, *Science,* **297,** 831–833.

Dickey, J.O., Marcus, S.L., de Viron, O. & Fukumori, I., 2002. Recent Earth oblateness variations: unraveling climate and postglacial rebound effects, *Science,* **298,** 1975–1977.

Dyurgerov, M., 2002. *Glacier Mass Balance and Regime Measurements and Analysis, 1945–2003 National Snow and Ice Data Center,* Boulder.

Enderlin, E.M., Howat, I., Jeong, S., Noh, M.-J., Van Angelen, J.H. & van den Broeke, M., 2014. An improved mass budget for the Greenland ice sheet, *Geophys. Res. Lett.,* **41,** 866–872.

Farrell, W.E. & Clark, J.A., 1976. On postglacial sea level, *Geophys. J. R. astr. Soc.,* **46,** 647–667.

Gutierrez, R. & Wilson, C.R., 1987. Seasonal air and water mass redistribution effects on LAGEOS and Starlette, *Geophys. Res. Lett.,* **14,** 929–932.

Han, D. & Wahr, J., 1995. The viscoelatic relaxation of a realisitically stratified Earth, and a further analysis of post-glacial rebound, *Geophys. J. Int.,* **120,** 287–311.

Jacob, T., Wahr, J., Pfeffer, W.T. & Swenson, S., 2012. Recent contributions of glaciers and ice caps to sea level rise, *Nature,* **482,** 514–518.

Lenaerts, J.T.M., van den Broeke, M.R., van Angelen, J.H., van Meijgaard, E. & Dery, S.J., 2012. Drifting snow climate of the Greenland ice sheet: a study with a regional climate model, *The Cryosphere,* **6,** 891–899.

Medley, B. *et al.*, 2013. Airborne-radar and ice-core observations of annual snow accumulation over Thwaites Glacier, West Antarctica confirm the spatiotemporal variability of global and regional atmospheric models, *Geophys. Res. Lett.,* **40,** 3649–3654.

Meehl, G.A., Arblaster, J.M., Matthes, K., Sassi, F. & van Loon, H., 2009. Amplifying the Pacific climate system response to a small 11-year solar cycle forcing, *Science,* **325,** 1114–1118.

Mouginot, J., Rignot, E. & Scheuchl, B., 2014. Sustained increase in ice discharge from the Amundsen Sea Embayment, West Antarctica, from 1973 to 2013, *Geophys. Res. Lett.,* **41,** 1576–1584.

Nerem, R.S. & Wahr, J., 2011. Recent changes in the Earth's oblateness driven by Greenland and Antarctic ice mass loss, *Geophys. Res. Lett.,* **38,** L13501, doi:10.1029/2011GL047879.

Rignot, E., Bamber, J., van den Broeke, M., Davis, C., Li, Y., van de Berg, W.J. & van Meijgaard, E., 2008a. Recent Antarctic ice mass loss from

radar interferometry and regional climate modelling, *Nat. Geosci.,* **1,** 106–110.

Rignot, E., Box, J.E., Burgess, E. & Hanna, E., 2008b. Mass balance of the Greenland ice sheet from 1958 to 2007, *Geophys. Res. Lett.,* **35,** L20502, doi:10.1029/2008GL035417.

Rodell, M. *et al.*, 2004. The global land data assimilation system, *Bull. Am. Meteor. Soc.,* **85,** 381–394.

Rui, H. & Beaudoing, H., 2013. *README Document for Global Land Data Assimilation System Version 2 (GLDAS-2) Products,* NASA's Goddard Space Flight Center, 22 pp.

Russell, C.T., Luhmann, J.G. & Jian, L.K., 2010. How unprecedented a solar minimum?, *Rev. Geophys.,* **48,** 1–16.

Sasgen, I. *et al.*, 2012. Timing and origin of recent regional ice-mass loss in Greenland, *EPSL,* **333–334,** 293–303.

Seo, K.-W., Waliser, D.E., Lee, C.-K., Tian, B., Scambos, T., Kim, B.-M., Van Angelen, J.H. & van den Broeke, M., 2015a. Accelerated mass loss from Greenland ice sheet: links to atmospheric circulation in the North Atlantic, *Global planet. Change,* **128,** 61–71.

Seo, K.-W., Wilson, C.R., Scambos, T., Kim, B.-M., Waliser, D.E., Tian, B., Kim, B.-H. & Eom, J., 2015b. Surface mass balance contributions to acceleration of Antarctic ice mass loss during 2003–2013, *J. geophys. Res.,* **120,** 3617–3627.

Simmons, A., Uppala, S., Dee, D. & Kobayashi, S., 2007. ERA-Interim: new ECMWF reanalysis products from 1989 onwards, ECMWF Newsletter No. 110.

Stammer, D., Ueyoshi, K., Köhl, A., Large, W.G., Josey, S.A. & Wunsch, C., 2004. Estimating air-sea fluxes of heat, freshwater, and momentum through global ocean data assimilation, *J. geophys. Res.,* **109,** C05023, doi:10.1029/2003JC002082.

van Angelen, J.H., Lenaerts, J.T.M., Lhermitte, S., Fettweis, X., Munneke, P.K., van den Broeke, M., van Meijgaard, E. & Greuell, W.G., 2012. Sensitivity of Greenland ice sheet surface mass balance to surface albedo parameterization: a study with a regional climate model, *Cryosphere,* **6**(5), 1175–1186.

van Wessem, J.M. *et al.*, 2014. Improved representation of East Antarctic surface mass balance in a regional atmospheric climate model, *J. Glaciol.,* **60,** 761–770.

Yoder, C.F., Williams, J.G., Dickey, J.O., Schutz, B.E., Eanes, R.J. & Tapley, B.D., 1983. Secular variations of Earth's gravitational harmonics J_2 coefficients from Lageos and nontidal acceleration of Earth rotation, *Nature,* **303,** 757–761.